Tungsten Nanowire Metamaterials as Selective Solar Thermal Absorbers by Excitation of Magnetic Polaritons

Jui-Yung Chang
School for Engineering of Matter, Transport, and Energy, Arizona State University, Tempe, AZ 85287

Hao Wang
School for Engineering of Matter, Transport, and Energy, Arizona State University, Tempe, AZ 85287

Liping Wang[1]
School for Engineering of Matter, Transport, and Energy, Arizona State University, Tempe, AZ 85287
e-mail: liping.wang@asu.edu

The present study focuses on nanowire-based metamaterials selective solar absorbers. Finite-difference time-domain (FDTD) simulation is employed for numerically designing a broadband solar absorber made of lossy tungsten nanowires which exhibit spectral selectivity due to the excitation of magnetic polariton (MP). An inductor–capacitor circuit model of the nanowire array is developed in order to predict the resonance wavelengths of the MP harmonic modes. The effects of geometric parameters such as nanowire diameter, height, and array period are investigated and understood by the sweep of geometric parameters, which tunes the MP resonance and the resulting optical and radiative properties. In addition, the optical properties and conversion efficiency of this nanowire-based absorber are both demonstrated to be insensitive on incidence angles, which illustrates the potential applicability of the proposed nanowire-based metamaterial as a high-efficiency wide-angle selective solar absorber. The results show that the nanowire-based selective solar absorber with base geometric parameters can reach 83.6% of conversion efficiency with low independence of incident angle. The results will facilitate the design of novel low-cost and high-efficiency materials for enhancing solar thermal energy harvesting and conversion. [DOI: 10.1115/1.4034845]

Keywords: nanowires, metamaterial, solar absorber, magnetic polariton

1 Introduction

Solar energy is sustainable, clean, and abundant. However, the performance of solar absorbers not only relies on broadband high absorptance within the solar spectrum but also the low thermal emission loss at longer wavelengths. Therefore, solar absorbers with spectral selectivity are highly desired to enhance the solar-to-heat conversion efficiency. Tailoring the radiative properties by constructing artificial micro/nanostructures or metamaterials has become a hot topic in recent years, and a variety of applications in energy harvesting, biosensing, and imaging have been found [1–4]. Excitation of magnetic polariton (MP) is one fundamental mechanism to obtain exotic radiative properties within metamaterials [5–7]. MP refers to the coupling between incident electromagnetic wave and internal magnetic resonance inside the structure, and its excitation has been widely investigated for 1D and 2D gratings, disk arrays, cross bars, and ring array structures [5,8,9]. On the other hand, metamaterials made of vertically aligned nanowire arrays have been extensively studied in aspect of negative refraction, selective absorbers, and emitters [10,11]. Effective medium approximation has been employed to investigate nanowire-based hyperbolic metamaterials, which has been demonstrated to have good agreement with full-wave numerical simulations [12]. However, effective medium theories (EMT), which approximate the inhomogeneous nanowire arrays as a homogeneous medium with effective dielectric functions or electric permittivities, only consider the response to the electric field. The validity of the effective medium theories would become questionable, and it needs to be reconsidered if magnetic resonance could be excited inside nanowire-based metamaterials, which has not been well understood.

In this work, we will employ the finite-difference time-domain (FDTD) method to numerically study the optical and radiative properties of vertically aligned tungsten nanowires sitting on a tungsten thin film, which can potentially serve as an efficient selective solar thermal absorber. Resonance behaviors within the tungsten nanowire structures are observed in the short wavelengths, leading to enhanced solar absorption, while reflective nature of tungsten in the IR leads to a high reflectance in that spectral region. More importantly, nanowire arrays are advantageous over multilayers that suffer from thermal stress issue and submicron periodic grating metamaterials whose large-area fabrication is prohibited. A comparison will first be made between the radiative properties obtained by the EMT and the FDTD simulation, in order to check the validity of EMT when MP is excited inside nanowire-based metamaterials. Furthermore, the electromagnetic field distribution at the resonance wavelengths will be presented, which clearly shows the exact MP behaviors of different modes. Moreover, an analytic inductor–capacitor (LC) circuit model will be introduced based on the electromagnetic field distribution to quantitatively predict the resonance wavelength of MP, further confirming the excitation of MP from the comparison with the FDTD simulation. The study on the geometric effects such as unit cell period, nanowire diameter, and nanowire height will be performed as well in order to fully understand the MP behavior in nanowire-based metamaterials. In addition, the incidence angle dependency on the optical properties and the conversion efficiency of the nanowire-based absorber will also be studied.

[1]Corresponding author.

Presented at the 2016 ASME 5th Micro/Nanoscale Heat & Mass Transfer International Conference. Paper Number MNHMT2016-6471.

Contributed by the Heat Transfer Division of ASME for publication in the Journal of Heat Transfer. Manuscript received February 3, 2016; final manuscript received June 20, 2016; published online February 7, 2017. Assoc. Editor: Zhuomin Zhang.

2 Structure Design, Numerical Method, and Effective Medium Theory

2.1 Designed Structures and Numerical Methods. As illustrated in Fig. 1, the selective solar absorber is constructed by vertically aligned tungsten nanowire array deposited on a tungsten thin film. Geometric parameters P, D, and H represent the array period, nanowire diameter, and height, respectively. The directions of electric field and magnetic field of a transverse magnetic (TM or p polarized) wave at normal incidence are also illustrated in the figure, respectively, by **E** and **H**. Note that, for normal incidence, the radiative properties of the selective absorber such as spectral absorptance under different polarized waves will be the same due to the geometric symmetry of nanowires. The tungsten thin film substrate will be considered as optically opaque as its thickness is set to be 500 nm.

Radiative properties of the designed selective solar absorber were obtained by FDTD method (Lumerical Solutions, Inc., Canada) within the wavelength range between 0.3 μm and 4 μm with 200 data points. Here, excellent numerical convergence is ensured by comparing the results with those obtained from 1851 wavelength points (i.e., a 2 nm interval). The optical property of tungsten is obtained from Palik's tabular data and assumed to be independent of temperature [13]. A plane-wave source with 0 deg polarization angle (TM wave as illustrated in Fig. 1) is placed above the absorber. Bloch boundary conditions which account for phase shifts between each period are established on both x and y directions for simulating periodic structures, while perfectly matched layers were set on z direction to avoid wave reflections from simulation domain boundaries. A minimum mesh size of 4 nm is used with nonuniform meshing, while the numerical error is less than 0.5% compared to the simulation using a minimum element size of 3 nm. Since the tungsten thin film substrate is thick enough to be opaque, the spectral absorptance α_λ of the selective absorber can then be obtained as $\alpha_\lambda = 1 - R_\lambda$ with R_λ obtained from a frequency-domain field and power monitor located above the plane-wave source.

2.2 Maxwell–Garnett Effective Medium Theory. An inhomogeneous nanowire array can be approximated as a homogeneous medium with widely used effective medium theories, which are homogenization approaches based on field average method [14]. For small filling ratios $f = \pi D^2/(4P^2) < 0.5$ considered in this study, the Maxwell–Garnett EMT method gives the effective dielectric functions as [15]

$$\varepsilon_{\parallel,\text{eff}} = \frac{(\varepsilon_W + 1) + f(\varepsilon_W - 1)}{(\varepsilon_W + 1) - f(\varepsilon_W - 1)} \tag{1}$$

$$\varepsilon_{\perp,\text{eff}} = 1 + f(\varepsilon_W - 1) \tag{2}$$

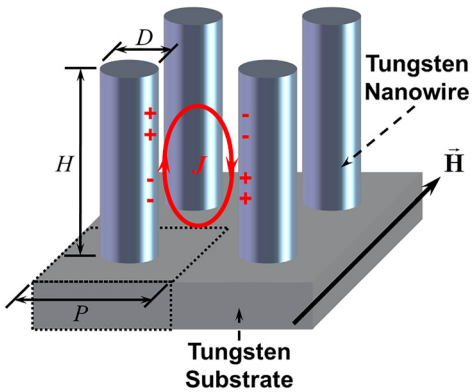

Fig. 1 Schematic of the tungsten nanowire-based selective absorber

where subscript W, (∥,eff), and (⊥,eff) denote tungsten, the parallel (in x–y plane), and vertical (out-of-plane) components of dielectric functions, respectively. Note that the variation of geometric parameters can only take effect by changing the filling ratio of the nanowire array. That is, the dielectric functions stay the same even with different array periods and nanowire diameters as far as the filling ratio is fixed.

3 Results and Discussion

3.1 Spectral Absorptance of the Selective Solar Absorber. In Sec. 2, two methods (i.e., FDTD and EMT) are introduced to acquire the radiative properties of the designed structure. Now, let us first compare the results obtained from EMT with the results from FDTD to check its validity as FDTD is a full-wave simulation which numerically solves the Maxwell equations in every mesh element. The geometric parameters of the selective solar absorber are set to be $D = 150$ nm, $P = 300$ nm, and $H = 600$ nm, which are used as base values to excite resonances within the solar spectrum. These geometric parameters are chosen considering the possibility of fabrication as well as the distinguishability of absorption peaks. The presented structure can be possibly fabricated by directional solidified eutectic NiAl–W alloy [16], while the tungsten substrate is sputtered before etching the NiAl host. As shown in Fig. 2(*a*), the spectral absorptance obtained from FDTD and EMT is different from each other in magnitude, while

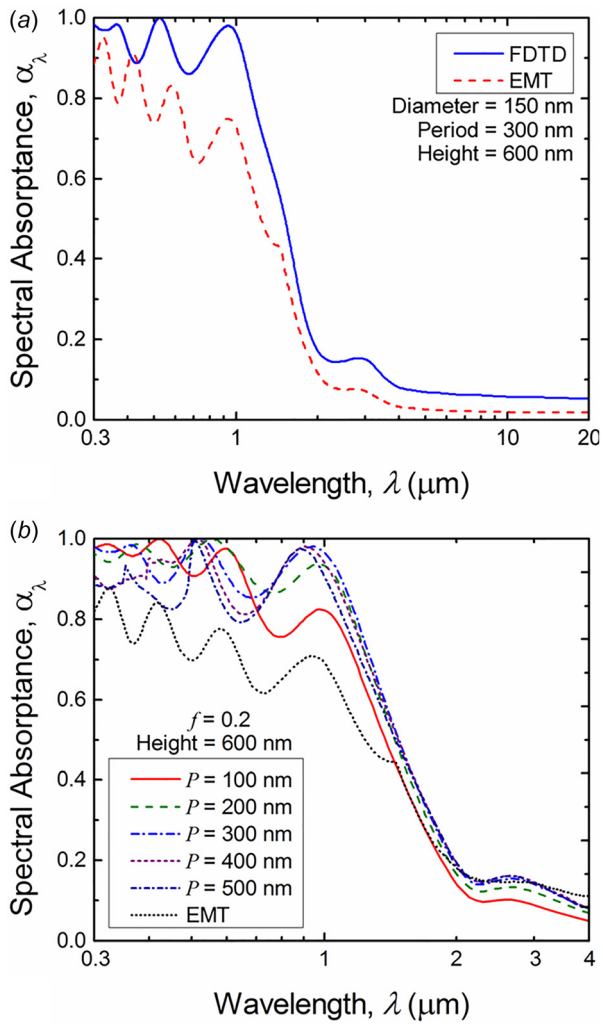

Fig. 2 The spectral absorptance of the selective absorber (*a*) based on FDTD simulation and EMT and (*b*) FDTD simulation with fixed filling ratio

the EMT could obtain similar oscillating resonance peaks but cannot accurately predict the absorptance in comparison with FDTD results. Due to the fact that the results of EMT calculation will not change under fixed filling ratio f, Fig. 2(*b*) illustrates the spectral absorptance with fixed f but different array periods and nanowire diameters in order to verify the accuracy of the results from EMT calculation. Clearly, the simulation result shows that the resonance peaks blue shift to shorter wavelengths when increasing the array period. On the other hand, EMT predicts the same spectral absorptance distribution with fixed f. Therefore, the EMT is proven to be inaccurate for predicting the optical response of considered tungsten nanowire structures. Furthermore, since EMT is a homogenization process which is not able to predict the resonance effects inside the material but only the bulk response, this can also show that the enhancement peaks are caused by resonance effects between the nanowires instead of the bulk responses of the structure, such as interference effect.

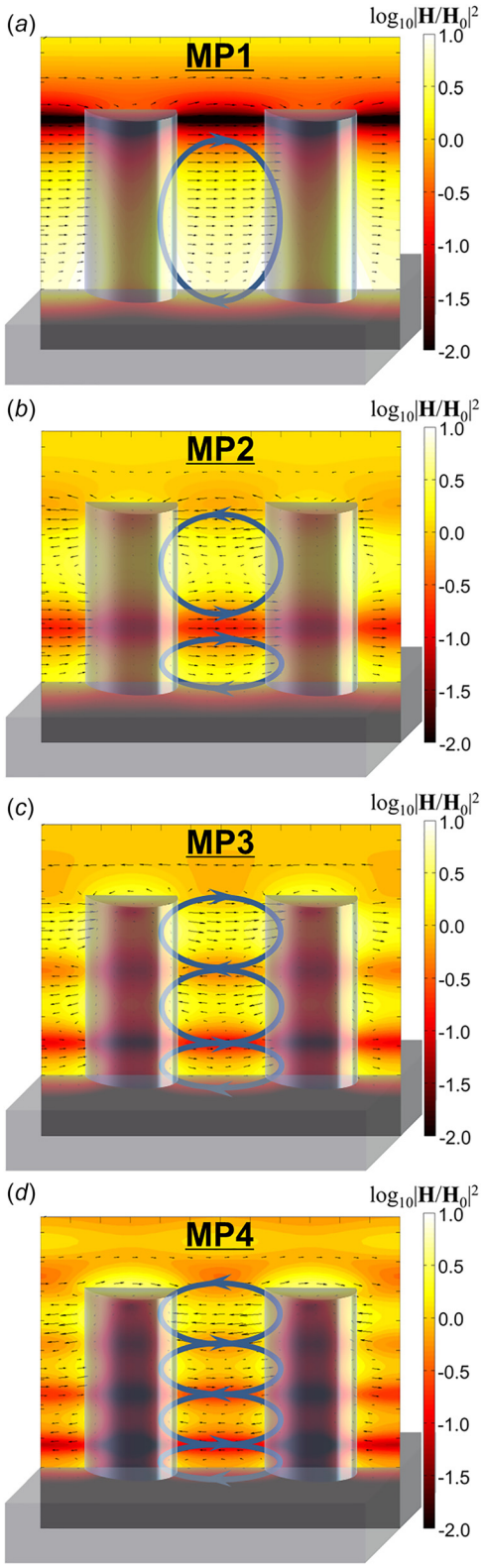

Fig. 3 The contour plots of electromagnetic field distribution on the *x–z* plane when MP resonances are excited at wavelengths of (*a*) 2.66 μm, (*b*) 0.93 μm, (*c*) 0.52 μm, and (*d*) 0.36 μm

3.2 Magnetic Polariton Between Nanowires. In order to understand the resonance effect indicated by spectral absorption peak, the electromagnetic field distributions are calculated by FDTD at resonance wavelengths: (a) 2.67 μm, (b) 0.93 μm, (c) 0.52 μm, and (d) 0.36 μm as shown in Fig. 3. The contour plots show the magnetic field normalized to the incident field, and the arrows represent the electric field vector. It can clearly be seen in Fig. 3(*a*) that there is a strong magnetic energy confinement between the nanowires. Furthermore, the electrical field vectors on both sides of the energy confinement are pointing at opposite directions (pointing down on right and up on left), while that inside the substrate points toward the left. This indicates that while the electric field forms a loop surrounding the confining region (the circle between nanowires). The similar behavior has been observed in grating-based metamaterials, which has been proven to be the resonance of MP [17]. When the excitation of MP is induced by the incident electromagnetic fields, an oscillating resonant electrical current caused by the free charges at the surface is generated inside the nanowire structures. The resonant electrical current loop oscillates between neighboring nanowires with strongly confined electromagnetic energy in the air gap, resulting in the enhancement of spectral absorptance/emittance at resonance wavelengths. Furthermore, higher harmonic modes of MP (i.e., MP2, MP3, and MP4) which contribute to the selective absorptance near visible range can also be obtained by FDTD simulation at shorter resonance wavelengths as shown in Figs. 3(*b*)–3(*d*). For the selective solar absorber, all the harmonic MP modes are very important to achieve high broadband absorption. Note that the surface plasmon polariton resonance cannot be excited in the visible range since the real part of tungsten permittivity is positive within the range.

3.3 An LC Circuit Model for Predicting MP Resonance Between Two Closely Spaced Thick Nanowires. As demonstrated by previous works [18–20], an analytical inductor–capacitor (LC) model based on surface charge distribution at MP resonance wavelength has been successfully used for predicting the resonance condition for grating-based metamaterials. However, one major challenge in developing the LC model is the difficulty to quantify the inductance and capacitance due to the curved nanowire surface. Here, we propose a modified LC model by simplifying the nanowires to an effective plate, based on the similar strongly localized magnetic field distributions. The LC circuit model between two closely spaced and vertically aligned nanowires is presented in Fig. 4(*a*), where the air gap between two neighboring nanowires forms a capacitor C_g, $L_{m,NW}$ is the mutual inductance between nanowires, and $L_{k,NW}$ and $L_{k,SUB}$ are the kinetic inductance contributed by the drifting electrons in nanowires and substrate, respectively. Therefore, the total impedance of the LC circuit can be expressed as

$$Z_{total} = i[\omega(2L_{m,NW} + 2L_{k,NW} + L_{k,SUB}) - (\omega C_g)^{-1}] \quad (3)$$

Thus, by zeroing the total impedance of the circuit, the MP resonance wavelength of the fundamental mode can be obtained as

$$\lambda = 2\pi c\sqrt{C_g(2L_{m,NW} + 2L_{k,NW} + L_{k,SUB})} \quad (4)$$

Now, the challenging part of constructing the LC circuit model is to quantify the capacitance and inductances due to the curvy surface of the nanowire. Considering that the LC circuit model is a simple estimation method, it would not be worthwhile to integrate the parameters over the circular nanowire surfaces and end up with complicated expressions, which would defeat the purpose of the LC model. Instead, we chose to simplify the problem by approximating the nanowires as effective parallel plates with spacing in between, setting the nonuniform charge distribution factor c_1 as 0.4, and setting the effective penetration depth δ_{eff} as $3\delta_W$ based on the electromagnetic field distribution. In this way, all the formulae of capacitance and inductance for deep gratings, which can be found in Refs. [19–21] and will not be repeated here, can be directly adopted for nanowires as effective parallel plates.

Figure 4(*b*) reveals the electromagnetic field distribution in *x*–*y* plane located at 0.3 μm above the bottom of the nanowires (i.e., at the middle of the nanowires) when MP1 resonance is excited (2.66 μm). Based on the strength of the magnetic field, the effective penetration depth δ_{eff} within the effective plates is thereby taken as three times of that within the bulk tungsten, which is $\delta_W = \lambda/4\pi\kappa$ with κ being the wavelength-dependent extinction coefficient. The capacitance and the inductance are then calculated by the geometric parameters of the effective plates according to the LC circuit model for deep gratings [17,21]. As a result, the resonance wavelength of MP1 on the base geometry predicted by the LC circuit model is 2.82 μm compared to 2.66 μm obtained from FDTD simulation with 6% relative error, confirming that the resonance is actually due to excitation of magnetic resonance.

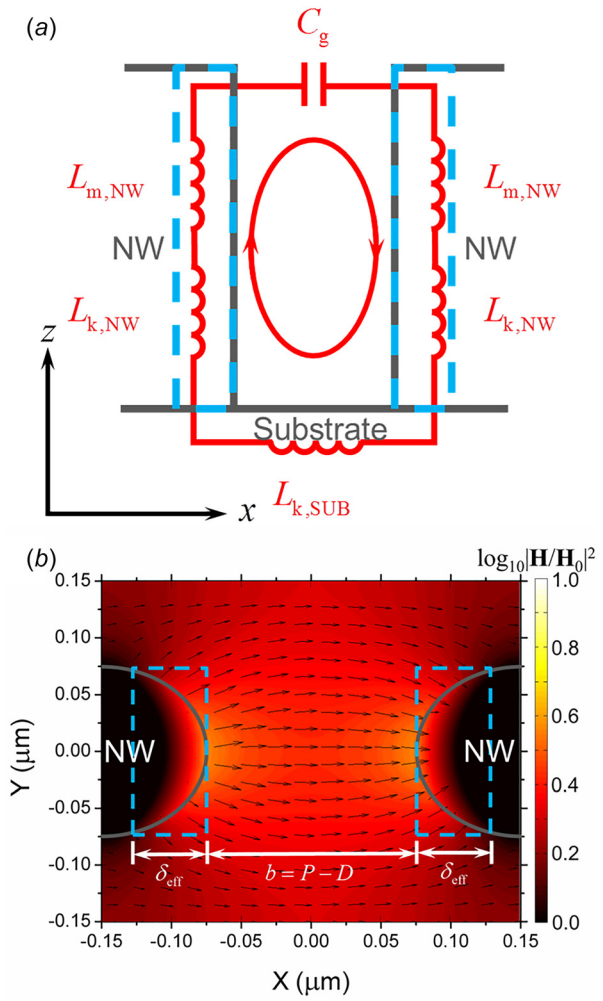

Fig. 4 (*a*) The LC circuit model based on charge and field distribution and (*b*) the electromagnetic field distribution on the *x*–*y* plane located at 0.3 μm above the bottom of the nanowires when MP is excited at 2.66 μm in wavelength

3.4 Geometric Effects on Spectral Absorptance. The main goal of the study is to achieve selective spectral absorptivity for efficient solar absorbers. In other words, near-unity absorptance in the solar spectrum and near-zero spectral emittance/absorptance (spectral absorptance = spectral emittance according to Kirchhoff's law) in the infrared regime are required. One of the most beneficial features of MP resonance is the tunability provided by geometric parameters as illustrated in Fig. 5. As shown in Fig. 5(*a*), the spectral absorptance peaks at MP resonances blue shift to shorter wavelengths (where most of the solar energy is distributed) when increasing the array period and fixing the diameter and height. Meanwhile, the amplitude of the enhancement peaks at shorter wavelengths also increased to near-unity. On the other hand, the resonance peak of MP1 is suppressed which is opposite to higher harmonic modes under larger array period. All these phenomena would benefit the design of selective solar absorber.

Figure 5(*b*) indicates that increasing nanowire diameter or decreasing the air gap under fixed *P* and *H* leads to opposite trend of spectral absorptance tunability as it results in smaller air gap. Both the red shifting and the increase of magnitude of the resonance peaks can clearly be observed. However, the higher harmonic terms of MP resonance maintains red shifting but again a reverse trend of the enhancement strength occurs. This is due to the fact that with a smaller air gap, energy can be better confined between neighboring nanowires under higher harmonic terms of MP resonance. Figure 5(*c*) shows the effect of nanowire height on spectral absorptance with both *P* and *D* fixed. The blue shifting of resonance peaks is clear, but the tunability of *H* on spectral absorptance enhancement is not that obvious. Furthermore, the effect of high harmonic resonance terms cannot be seen as the nanowires are too short. Note that, when it comes to fabrication process, the uncertainties of fabrication might lead to the shifting of enhancement peaks as shown in Fig. 5. More specifically, an uncertainty at the order of tens of nanometer on either period or diameter will lead to slight shift of the resonance peaks which will little affect the performance of the absorber. On the other hand, the uncertainty on nanowire height will affect the performance significantly when it is on the order of micrometer.

The resonance wavelengths of MP1 with different geometric parameters obtained by FDTD simulation are also compared with that predicted by LC circuit model. As shown in Fig. 6(*a*), the blue shift of resonance wavelength with increasing unit cell period can clearly be seen, while the result of LC circuit model also presents the same trend. As for the effects of nanowire diameter and height as shown in Figs. 6(*b*) and 6(*c*), similar trends are also observed which can further verify the accuracy and rationality of the LC circuit model presented in this study.

3.5 Effect of Incidence Angle. As for the practicability of a selective solar absorber without tracing devices under sunlight (considered as randomly polarized or unpolarized wave), the dependence of incidence angle is also important and need to be studied. Figures 7(*a*) and 7(*b*) illustrate the incident angle dependence of the spectral absorptance at MP2 and MP3, respectively, for TE and TM waves. The two wavelengths (0.93 μm for MP2 and 0.52 μm for MP3) are selected since these two enhancement peaks are the main resonance that can be tuned to the visible regime by geometric parameters. As shown in Fig. 7, for both TE and TM waves, these two resonance peaks show great independency for incidence angles up to ±60 deg. That is, the spectral absorptance can still reach about 0.8 at ±60 deg for TE waves and

even at ±75 deg for TM waves. Furthermore, both peaks maintain at above 0.9 within ±30 deg for TE waves and ±45 deg for TM waves. This can greatly reduce the cost of selective solar absorbers by providing large clearance on tracking devises or even using them for nontracking solar absorbers. Note that the spectral absorptance of both wavelengths shows small spikes at large incident angle under TE waves but not TM waves. This is due to the fact that for TM waves, the direction of magnetic field (i.e., y direction) is independent of incident angle, which is contrary to the case for TE waves. MP resonance strength becomes weaker

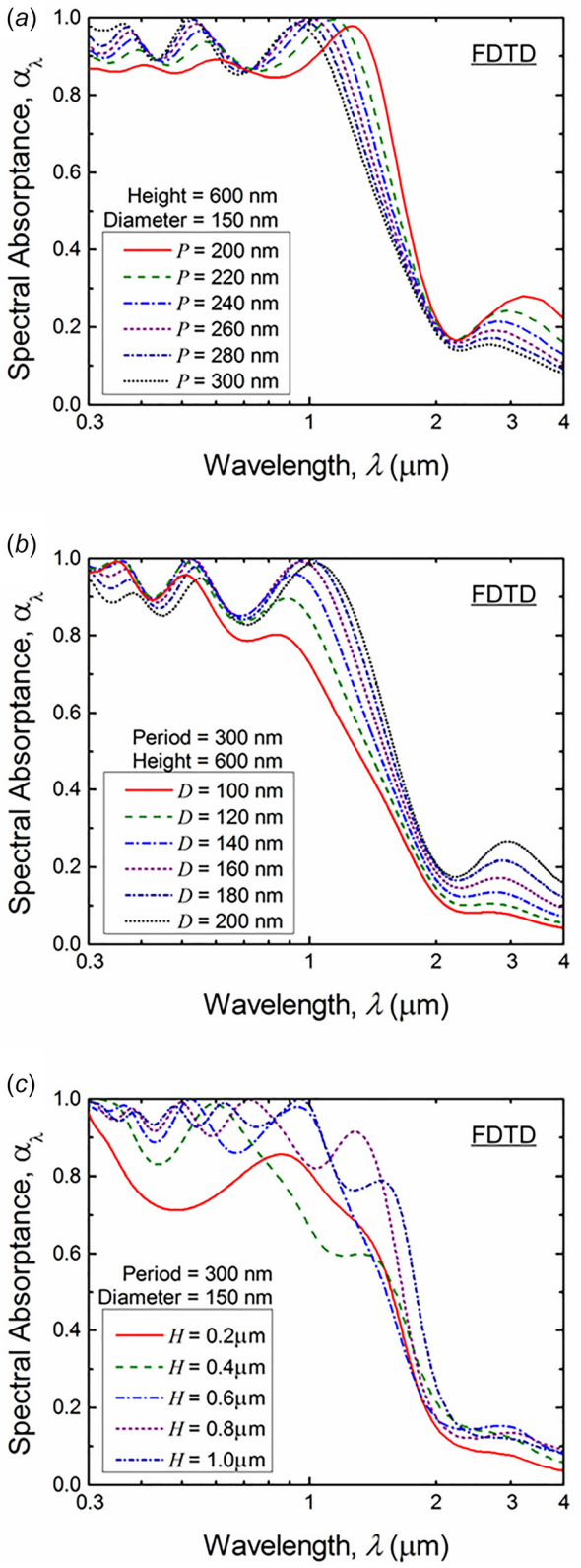

Fig. 5 The spectral absorptance with respect to different nanowires: (*a*) array period, (*b*) diameter, and (*c*) height simulated by FDTD

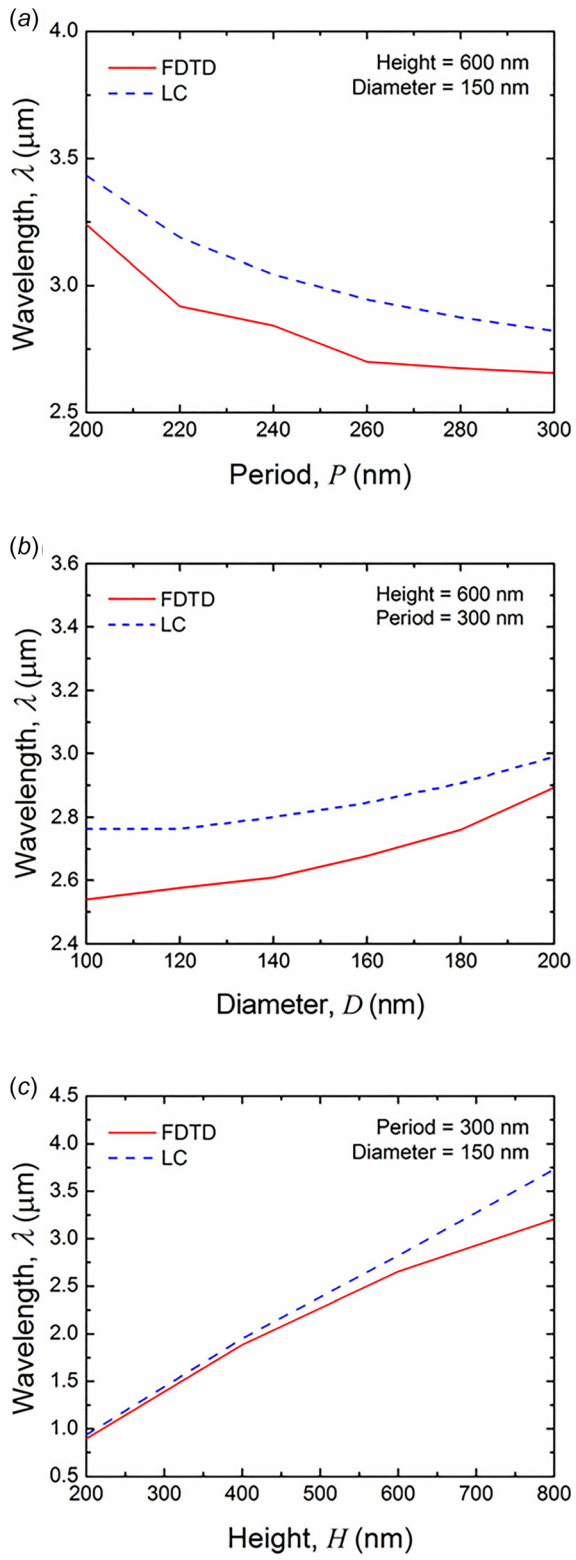

Fig. 6 The MP1 wavelengths predicted by FDTD and LC circuit model with respect to different nanowires: (*a*) array period, (*b*) diameter, and (*c*) height

under large incident angle for TM waves since electrical field that forms the resonance current loop becomes weaker; however, for TE waves, the direction of magnetic field changes and thus instead of forming an electrical current loop in x–z plane, the loop is formed in x–y plane between the two neighboring nanowires.

Figure 7(*c*) reveals the spectral absorptance at MP2 and MP3 for unpolarized waves, which indicates solar incidence. This further proves that the selective solar absorber has high spectral absorptance with low incident angle dependence at the resonance wavelengths of interest. Note that the spectral absorptance is independent of wave polarization angle at normal incidence due to the geometric symmetry of nanowires as mentioned previously (i.e., 2D periodic structure with same parameters).

3.6 Performance Analysis. After confirming that the resonance effect is independent of incident angle, the conversion efficiency of the nanowire-based selective absorber will then be presented. Here, since the main goal of this study is to verify the mechanism and show the potential of achieving selective absorptance by nanowire structures, the performance analysis performed here will not be optimized with geometric parameters. That is, the performance analysis will only be carried out by the base geometry. The conversion efficiency is obtained through [17]

$$\eta = \frac{\alpha_{\text{total}} CG - \varepsilon_{\text{total}} \sigma \left(T_{\text{A}}^4 - T_{\text{sky}}^4\right)}{CG} \tag{5}$$

where

$$\alpha_{\text{total}} = \frac{\int_{0.3\mu\text{m}}^{4\mu\text{m}} \alpha_{\lambda,N} I_{\text{AM1.5}}(\lambda) d\lambda}{\int_{0.3\mu\text{m}}^{4\mu\text{m}} I_{\text{AM1.5}}(\lambda) d\lambda} \tag{6}$$

and

$$\varepsilon_{\text{total}} = \frac{\int_{0.3\mu\text{m}}^{20\mu\text{m}} \varepsilon_{\lambda,N} I_{\text{BB}}(\lambda, T_{\text{A}}) d\lambda}{\int_{0.3\mu\text{m}}^{20\mu\text{m}} I_{\text{BB}}(\lambda, T_{\text{A}}) d\lambda} \tag{7}$$

Here, C is the concentration factor of sun light, and T_{A} is the absorber temperature. The constants sky temperature T_{sky} and incidence heat flux of solar irradiation G (AM1.5 is assumed) are kept to be 273 K and 1000 W/m^2, respectively. Figure 8(*a*) first shows the conversion efficiencies of four different absorbers with respect to different absorber temperature under one sun. The ideal absorber assumes unity absorptance and zero emittance with an optimal cutoff wavelength, and the blackbody absorber assumes

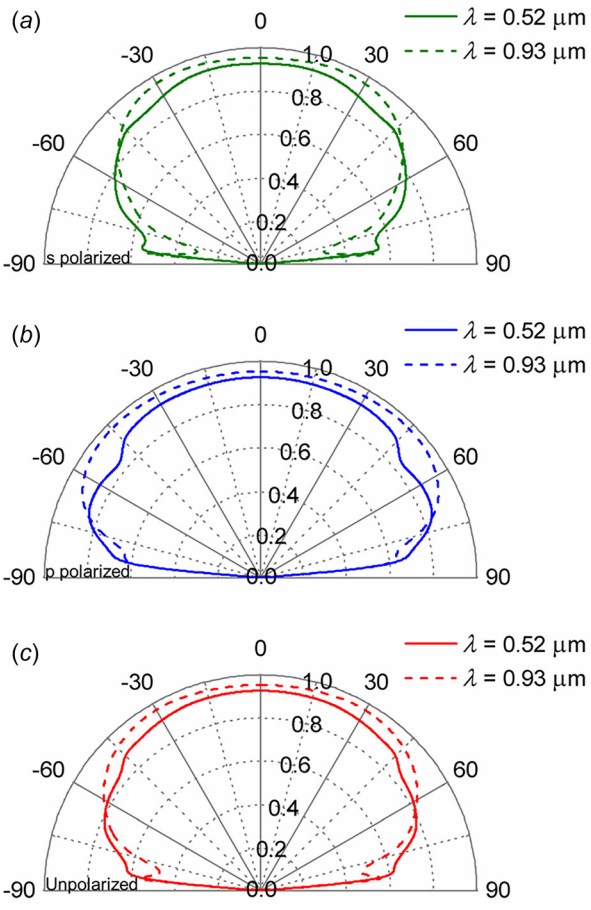

Fig. 7 The spectral absorptance at two resonance frequencies (MP2 and MP3) as a function of incident angle under (*a*) s-polarized, (*b*) p-polarized, and (*c*) unpolarized waves

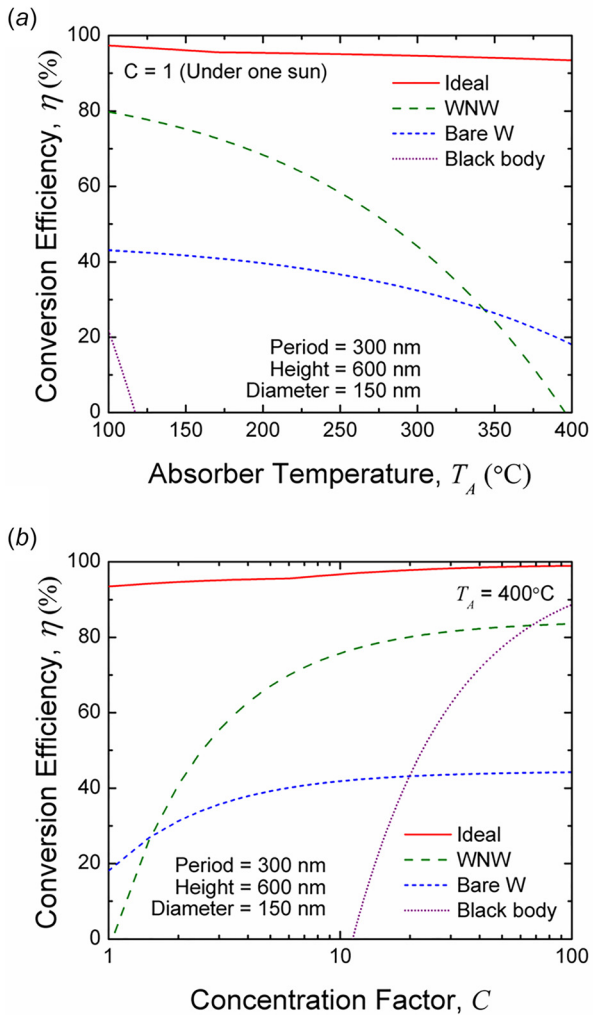

Fig. 8 The comparison of conversion efficiencies between ideal, nanowire-based, bare tungsten, and blackbody absorbers with different (*a*) absorber temperatures and (*b*) concentration factors

unity absorptance/emittance throughout the whole spectrum. As shown in the figure, ideally the conversion efficiency can reach about 95%, but only the nanowire-based absorber can reach ~80% efficiency at 100 °C while the two absorbers made of bare tungsten (~43.1%) and blackbody (~21.7%) are both far below that. However, as the absorber temperature rises, the efficiency of nanowire-based absorber drops much faster than that of bare tungsten absorber. This is due to the fact that the nanowire absorber has a broader absorption/emission band which extends to the near infrared. Although the efficiencies of the two absorbers are about the same when the absorber temperature reaches 350 °C and the nanowire-based absorber performs even worse with further increasing temperature, this does not mean the absorber is only applicable for low temperature conditions. In fact, as shown in Fig. 8(*b*) while the absorber temperature is fixed at 400 °C, the nanowire-based absorber works much efficiently as long as the concentration factor is above 1.6. Note that, due to the unity absorptance throughout the whole spectrum, the efficiency of blackbody absorber increases rapidly under high concentration factor.

4 Conclusion

In summary, we have designed a nanowire-based metamaterial as a broadband selective absorber for solar energy harvesting systems. With FDTD simulation, the radiative properties of selective absorber were investigated. In comparison with the FDTD results, the EMT fails to predict the MP resonance and the absorption peaks accurately. The selective absorption is realized by the excitation of multiple harmonic MP modes between nanowires. The underlying physical mechanism has been explained by the LC circuit and EM field distribution. By tuning the geometric parameters, the MP resonance could occur at desired wavelengths for different purposes. On the other hand, the incident angle independency of the selective solar absorber is also demonstrated. In addition, the performance analysis also shows that the conversion efficiency of the nanowire-based absorber exceeds that of bare tungsten and blackbody absorbers under most conditions and can reach at most 83.58% when the concentration factor reaches 100. The results would facilitate the design of novel low-cost and high-efficiency materials for enhancing the solar energy harvesting and conversion.

Acknowledgment

The authors greatly appreciate the partial supports from the National Science Foundation (CBET-1454698), the Australian Renewable Energy Agency for the US-Australia Solar Energy Collaboration—Micro Urban Solar Integrated Concentrators Project, and the ASU New Faculty Startup Funds.

Nomenclature

C = concentration factor
C_g = gap capacitance (F)
D = nanowire diameter (m)
$\mathbf{E}$ = electric field vector (V/m)
f = filling ratio of metal nanowire
G = incidence heat flux of solar irradiation (W/m^2)
H = nanowire height (m)
$\mathbf{H}$ = magnetic field vector (A/m)
$I_{AM1.5}$ = spectral intensity of solar irradiation at AM1.5 (W sr^{-1} m^{-1})
I_{BB} = spectral intensity of a blackbody (W sr^{-1} m^{-1})
$L_{k,NW}$ = kinetic inductance of nanowire (H)
$L_{k,SUB}$ = kinetic inductance of substrate (H)
$L_{m,NW}$ = mutual inductance of nanowire (H)
P = nanowire array period (m)
T_A = absorber temperature (K)
T_{sky} = sky temperature (K)
Z_{total} = total impedance (Ω)

Greek Symbols

α_{total} = total absorptance
α_λ = spectral absorptance
δ_W = penetration depth of tungsten
δ_{eff} = effective penetration depth
ε_W = dielectric function (relative permittivity) of tungsten
ε_{total} = total emittance
$\varepsilon_{\parallel,eff}$ = effective dielectric function (relative permittivity) parallel to the substrate surface
$\varepsilon_{\perp,eff}$ = effective dielectric function (relative permittivity) vertical to the substrate surface
γ_λ = spectral reflectance
λ = wavelength (m)
σ = Stefan–Boltzmann constant (kg s^{-3} K^{-4})

Subscripts

A = absorber
AM1.5 = global tilt air mass 1.5 data
BB = blackbody
g = gap
k,NW = kinetic, nanowire
k,SUB = kinetic, substrate
m,NW = mutual, nanowire
sky = sky
total = total
W = tungsten
λ = spectral
$\parallel$,eff = direction parallel to the substrate surface, effective
$\perp$,eff = direction vertical to the substrate surface, effective

References

[1] Wang, L. P., and Zhang, Z. M., 2012, "Wavelength-Selective and Diffuse Emitter Enhanced by Magnetic Polaritons for Thermophotovoltaics," Appl. Phys. Lett., **100**(6), p. 063902.
[2] Zhao, B., Wang, L. P., Shuai, Y., and Zhang, Z. M., 2013, "Thermophotovoltaic Emitters Based on a Two-Dimensional Grating/Thin-Film Nanostructure," Int. J. Heat Mass Transfer, **67**, pp. 637–645.
[3] Sacchetto, D., Doucey, M.-A., De Micheli, G., Leblebici, Y., and Carrara, S., 2011, "New Insight on Bio-Sensing by Nano-Fabricated Memristors," BioNanoScience, **1**(1), pp. 1–3.
[4] Johnson, J. C., Yan, H. Q., Schaller, R. D., Petersen, P. B., Yang, P. D., and Saykally, R. J., 2002, "Near-Field Imaging of Nonlinear Optical Mixing in Single Zinc Oxide Nanowires," Nano Lett., **2**(4), pp. 279–283.
[5] Wang, L. P., and Zhang, Z. M., 2013, "Measurement of Coherent Thermal Emission Due to Magnetic Polaritons in Subwavelength Microstructures," ASME J. Heat Transfer, **135**(9), p. 091505.
[6] Sakurai, A., Zhao, B., and Zhang, Z. M., 2014, "Resonant Frequency and Bandwidth of Metamaterial Emitters and Absorbers Predicted by an RLC Circuit Model," J. Quant. Spectrosc. Radiat. Transfer, **149**, pp. 33–40.
[7] Zhao, B., Zhao, J. M., and Zhang, Z. M., 2014, "Enhancement of Near-Infrared Absorption in Graphene With Metal Gratings," Appl. Phys. Lett., **105**(3), p. 031905.
[8] Wang, L. P., and Zhang, Z. M., 2010, "Effect of Magnetic Polaritons on the Radiative Properties of Double-Layer Nanoslit Arrays," J. Opt. Soc. Am. B, **27**(12), pp. 2595–2604.
[9] Wang, L. P., Haider, A., and Zhang, Z. M., 2014, "Effect of Magnetic Polaritons on the Radiative Properties of Inclined Plate Arrays," J. Quant. Spectrosc. Radiat. Transfer, **132**, pp. 52–60.
[10] Liu, X. L., Wang, L. P., and Zhang, Z. M., 2013, "Wideband Tunable Omnidirectional Infrared Absorbers Based on Doped-Silicon Nanowire Arrays," ASME J. Heat Transfer, **135**(6), p. 061602.
[11] Liu, X. L., and Zhang, Z. M., 2013, "Metal-Free Low-Loss Negative Refraction in the Mid-Infrared Region," Appl. Phys. Lett., **103**(10), p. 103101.
[12] Chang, J.-Y., Yang, Y., and Wang, L. P., 2015, "Tungsten Nanowire Based Hyperbolic Metamaterial Emitters for Near-Field Thermophotovoltaic Applications," Int. J. Heat Mass Transfer, **87**, pp. 237–247.
[13] Palik, E. D., 1998, *Handbook of Optical Constants of Solids*, Academic Press, Cambridge, MA.
[14] Wang, H., Liu, X. L., Wang, L. P., and Zhang, Z. M., 2013, "Anisotropic Optical Properties of Silicon Nanowire Arrays Based on the Effective Medium Approximation," Int. J. Therm. Sci., **65**, pp. 62–69.
[15] Choy, T. C., 1999, *Effective Medium Theory: Principles and Applications*, Oxford University Press, Oxford, UK.

[16] Hassel, A. W., Smith, A. J., and Milenkovic, S., 2006, "Nanostructures From Directionally Solidified NiAl–W Eutectic Alloys," Electrochim. Acta, **52**(4), pp. 1799–1804.
[17] Wang, H., and Wang, L. P., 2013, "Perfect Selective Metamaterial Solar Absorbers," Opt. Express, **21**, pp. A1078–A1093.
[18] Lee, B. J., Wang, L. P., and Zhang, Z. M., 2008, "Coherent Thermal Emission by Excitation of Magnetic Polaritons Between Periodic Strips and a Metallic Film," Opt. Express, **16**(15), pp. 11328–11336.
[19] Wang, L. P., and Zhang, Z. M., 2009, "Resonance Transmission or Absorption in Deep Gratings Explained by Magnetic Polaritons," Appl. Phys. Lett., **95**(11), p. 111904.
[20] Zhao, B., and Zhang, Z. M., 2014, "Study of Magnetic Polaritons in Deep Gratings for Thermal Emission Control," J. Quant. Spectrosc. Radiat. Transfer, **135**, pp. 81–89.
[21] Wang, L. P., and Zhang, Z. M., 2011, "Phonon-Mediated Magnetic Polaritons in the Infrared Region," Opt. Express, **19**, pp. A126–A135.